Protein Structure and Folding:

The Peculiar Role of the A2V Mutation in Amyloid- β (Aβ) 1–42 Molecular Assembly

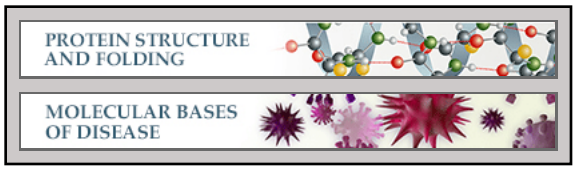

Massimo Messa, Laura Colombo, Elena del Favero, Laura Cantù, Tatiana Stoilova, Alfredo Cagnotto, Alessandro Rossi, Michela Morbin, Giuseppe Di Fede, Fabrizio Tagliavini and Mario Salmona

J. Biol. Chem. 2014, 289:24143-24152.
doi: 10.1074/jbc.M114.576256 originally published online July 18, 2014

THE JOURNAL OF BIOLOGICAL CHEMISTRY VOL. 289, NO. 35, pp. 24143–24152, August 29, 2014

The Peculiar Role of the A2V Mutation in Amyloid-β (Aβ) 1–42 Molecular Assembly*

Received for publication, May 5, 2014, and in revised form, July 11, 2014 Published, JBC Papers in Press, July 18, 2014, DOI 10.1074/jbc.M114.576256

Massimo Messa[‡], Laura Colombo[‡], Elena del Favero[§], Laura Cantù[§], Tatiana Stoilova[‡], Alfredo Cagnotto[‡], Alessandro Rossi[‡], Michela Morbin[¶], Giuseppe Di Fede[¶], Fabrizio Tagliavini[¶], and Mario Salmona[‡1]

From the [‡]Department of Molecular Biochemistry and Pharmacology, IRCCS-Istituto di Ricerche Farmacologiche Mario Negri, Via La Masa 19, 20156, Milan, Italy, [§]Department of Medical Biotechnology and Translational Medicine, University of Milan, V.le F.lli Cervi 93, 20090 Segrate, Italy, and [¶]Neurology V and Neuropathology, IRCCS Foundation "Carlo Besta" Neurological Institute, Via Celoria 11, 20133 Milan, Italy

Background: A2V mutation is associated with early onset AD-type dementia in homozygous individuals.
Results: A2V mutation leads to a peculiar kinetics of Aβ oligomerization.
Conclusion: The Aβ N-terminal region plays an important role in the molecular assembly.
Significance: in the homozygous condition the A2V mutation led to aggregation, whereas in the heterozygous state the evolution and kinetics of the aggregation process was hindered.

We recently reported a novel Aβ precursor protein mutation (A673V), corresponding to position 2 of Aβ1–42 peptides ($A\beta1-42_{A2V}$), that caused an early onset AD-type dementia in a homozygous individual. The heterozygous relatives were not affected as an indication of autosomal recessive inheritance of this mutation. We investigated the folding kinetics of native unfolded $A\beta1-42_{A2V}$ in comparison with the wild type sequence ($A\beta1-42_{WT}$) and the equimolar solution of both peptides ($A\beta1-42_{MIX}$) to characterize the oligomers that are produced in the early phases. We carried out the structural characterization of the three preparations using electron and atomic force microscopy, fluorescence emission, and x-ray diffraction and described the soluble oligomer formation kinetics by laser light scattering. The mutation promoted a peculiar pathway of oligomerization, forming a connected system similar to a polymer network with hydrophobic residues on the external surface. $A\beta1-42_{MIX}$ generated assemblies very similar to those produced by $A\beta1-42_{WT}$, albeit with slower kinetics due to the difficulties of $A\beta1-42_{WT}$ and $A\beta1-42_{A2V}$ peptides in building up of stable intermolecular interaction.

Alzheimer disease (AD)[2] is the most common form of dementia in the elderly accounting for up to 30 million cases worldwide, a figure that is predicted to double in 20 years (1). AD neurodegeneration is characterized by extensive neuronal atrophy especially in hippocampus and cerebral cortex, whereas neuropathology detects neuronal and synapse loss in association with the deposition of amyloid plaques and neurofibrillary tangles (2).

Amyloid plaque presents a core composed of misfolded amyloid β (Aβ) peptides of 37–43 amino acid lengths in the form of oligomers and amyloid fibrils. One of the pathogenic hypotheses to explain AD considers these aggregated Aβ species, particularly the soluble oligomers of Aβ but not monomers or insoluble amyloid fibrils (3–6), to be the ultimate molecular triggers of a cascade of events (amyloid cascade) leading to synaptotoxicity and causing the observed neuronal loss (7). In fact there are several pieces of evidence that correlate Aβ peptide with the pathological mechanism of AD, suggesting that Aβ occupies a crucial position in the etiopathology. The most abundant peptides are Aβ1–40 and Aβ1–42, the first being the prevalent fragment and the second the most amyloidogenic (8). The aggregation of Aβ peptides starts with changes in their secondary structure leading to β-sheet formation, it progresses with aggregation of the misfolded peptides into oligomers, and it culminates in the production of amyloid fibers that precipitate into the brain forming amyloid plaques. Synthetic Aβ peptides are used to reproduce *in vitro* oligomeric structures, thus enabling the study of their features. The oligomers that have been described so far are paranucleus (5-nm diameter) (9), Aβ-derived diffusible ligands (~53 kDa), synthetic analog of Aβ*56 (3, 10), AβO (~90 kDa, 15–20-mer) (11), protofibrils (24–700-mer) (8), annular assemblies (150–250 kDa) (12, 13), amylospheroid (~150–700 kDa) (14), and βamyball (50–100-μm diameter spheroids) (15). These oligomeric species differ by size and shape, and they can be both on- or off-pathway intermediates (15); however, all of them are able to dynamically assemble and progress to more aggregated states contributing to the growth and maturation of amyloid fibers.

A large body of literature confirms the importance of the Aβ sequence region spanning residues 21–30 in the molecular assembly (16–24). This is a central hydrophobic core resistant to protease degradation, and the prediction of its importance in the determination of the aggregation tendency of Aβ peptides has been confirmed by the experimental analysis of Aβ peptides containing the Arctic (E22G), Dutch E22Q), and Iowa (D23N) mutations, all characterized by high propensity to form amyloid

* This work was supported by the Italian Ministry of Health (RF-2009-1473239), Banca Intesa Sanpaolo Grant 2012-2013, and Ministero dell'Istruzione dell'Università e della Ricerca Grant RBAP11FRE9.
[1] To whom correspondence should be addressed. Tel.: 39-0239014447; Fax: 39-0239014744; E-mail: mario.salmona@marionegri.it.
[2] The abbreviations used are: AD, Alzheimer disease; Aβ, amyloid-β; AFM, atomic force microscopy; LLS, laser light scattering; SLS, static laser light scattering; DLS, dynamic laser light scattering; SAXS, small angle x-ray scattering; ANS, 1-anilino-8-naphthalene-sulfonate; Bis-ANS, 4,4′-dianilino-1,1′-binaphthyl-5,5′-disulfonic acid.

fibrils (20, 25). Recently Scheidt *et al.* (26) demonstrated that the three-four amino acid residues at the N terminus of the Aβ region also play an important role in the formation of a stable β-sheet secondary structure in the Aβ peptide. Familial AD forms are linked to mutations in presenilin 1, presenilin 2, or in amyloid precursor protein genes and usually show an autosomal pattern of inheritance with total penetrance (27). In 2009 we described a new amyloid precursor protein mutation (A673V) that causes early onset AD when in homozygosity. The missense mutation consists of a C-to-T transition resulting in an alanine-to-valine substitution at position 673 of amyloid precursor protein that corresponds to position 2 of Aβ1–40 and Aβ1–42 peptides (Aβ A2V peptides). Notably, heterozygous individuals do not develop AD even in advanced age. In fact, five A673V heterozygous performed well on the neuropsychological assessments, and in particular, the 88-year-old aunt of the proband showed excellent performance on all the tests despite the fact that she was non-educated. The amyloid plaques and neurofibrillary tangles, the cardinal features of AD, were thought to underlie this chronic neurological disorder. Even today, after several years of research on AD, the Aβ peptides play a central role in the onset, development, and exacerbation of the AD in all of its forms of aggregation. However, the emerging soluble Aβ oligomers are now widely recognized as key pathogenic structures in AD (28, 29). In fact, in light of recent findings and the realization that the amyloid cascade theory is insufficient to explain Alzheimer pathology, the amyloid hypothesis has been updated, as fibrils were considered the first and only species leading to AD pathogenesis (30). Recently, Aβ oligomers were identified as the main cause of synaptic dysfunction leading to alterations in both neuronal activity and cognitive function (31).

In this study we generated Aβ1–42 oligomers from peptides spanning the wild type or the A2V sequences. Oligomers were produced from solutions of pure Aβ1–42$_{WT}$, Aβ1–42$_{A2V}$, and the equimolar solution of both (Aβ1–42$_{MIX}$). This enabled us to investigate the structure and the formation of toxic oligomeric species. Moreover, we conducted a comparative chemico-physical study on Aβ1–42$_{WT}$, Aβ1–42$_{A2V}$, and Aβ1–42$_{MIX}$ molecular assembly to describe features of different oligomeric populations produced in the early phase of the oligomerization process. This revealed the influence of the A2V mutation in Aβ1–42 folding and produces evidence for the toxicity of Aβ1–42 and the protective effect displayed by the Aβ1–42$_{MIX}$. Finally, the position of the A2V mutation in the N terminus of Aβ peptides definitely strengthens the relevance of this region for peptide structure and spatial shape re-arrangement.

EXPERIMENTAL PROCEDURES

Peptide Synthesis and Sample Preparation—Aβ1–42 peptides were synthesized using depsipeptide method as previously described (32–35). Aβ1–42$_{WT}$ and Aβ1–42$_{A2V}$ were stored in acidic solution (water:trifluoroacetic acid, 0.02%) at a concentration of ~200 μM. The depsipeptide method is a specific technique of synthesis used for amyloidogenic difficult sequences, and it allow us to obtain a batch with a low degree/level of aggregation free of either highly folded structures or fibrils and aggregates (seeds free) and as close as possible to monomeric conditions. In the case of Aβ1–42, the method consists of introducing an *O*-acyl isopeptide structure into the Gly-25–Ser-26 sequence, stable at acidic pH and able to inhibit the self-aggregation. Upon a change to basic pH (switching procedure), the peptide is converted to the Aβ1–42 native sequence. Before the switching procedure to minimize the pre-aggregated species and to obtain the best reproducibility, peptides were dissolved in acidic solution (water, 0.02% trifluoroacetic acid) and clarified overnight (16–18 h) at 55,000 rpm to obtain seeds-free samples, filtered on a Microcon (centrifugal filter devices, cutoff 10 kDa, Millipore), and finally, concentrated on a Microcon (centrifugal filter devices, c.o. 3 kDa, Millipore) up to a concentration of ≥200 μM. The switching procedure of depsipeptide Aβ was carried out at basic pH; a mix of sodium hydroxide (NaOH) and ammonium hydroxide (NH_4OH) (ratio 3:1) was added to the peptide solutions (final pH of ~10) and incubated on ice for 10–15 min. The preparation of MIX was done by adding an equimolar solution of both peptides before the switching procedure to obtain a Aβ1–42 peptide mixture with a concentration of ~200 μM constituted by ½ Aβ1–42$_{WT}$ and ½ Aβ1–42$_{A2V}$. Oligomers were prepared using the following procedure; after the switching procedure, Aβ1–42 solutions were brought to a final concentration of 100 μM in 50 mM phosphate buffer, pH 7.4, and incubated for 24 h at 4 or 22 °C to obtain oligomer-rich preparations (36, 37).

Electron Microscopy (EM)—EM was used to investigate the structure of the peptide aggregates. 10 μl of Aβ1–42 oligomer preparations (Aβ1–42$_{WT}$, Aβ1–42$_{A2V}$, and Aβ1–42$_{MIX}$) were dropped onto 300-mesh Formvar/carbon nickel grids (Electron Microscopy Science), and after 5 min the solution was removed. Samples were counterstained for 5 min with saturated solution of uranyl acetate, washed with MilliQ water to eliminate excess uranyl acetate, and allowed to air dry (38, 39). EM analyses were performed with a Libra 120 apparatus operating at 120 kV equipped with a Proscan Slow Scan CCD camera (Carl Zeiss).

Atomic Force Microscopy (AFM)—AFM was carried out on a Multimode AFM with a Nanoscope V system operating in tapping mode using standard phosphorus-doped silicon probes (thickness range, 3.5–4.5 μm; length, 115–135 μm; width, 30–40 μm; spring constant, 20–80 newtons/m, Veeco/Digital Instruments) with a scan rate in the 0.5–1.2 Hz range, proportional to the area scanned. Freshly cleaved muscovite mica discs (Veeco/Digital Instruments) were used for deposition of peptide samples. Aβ1–42 oligomeric solutions were added to freshly cleaved mica at room temperature for 1 min and, then the samples were washed and dried under gentle nitrogen flow. AFM images of Aβ1–42 samples were analyzed for diameter and height with the Scanning Probe Image Processor (SPIP Version 5.1.6 (released April 13, 2011) data analysis package to describe oligomer structures. To exclude the interference of possible artifacts, extra control samples, such as freshly cleaved mica and freshly cleaved mica soaked with ultra-pure water, were also used. All the topographic patterns and SPIP characterization described in the text were confirmed by additional measurements in a minimum of 10 different, well separated areas.

Laser Light Scattering (LLS)—Aβ1–42$_{WT}$, Aβ1–42$_{A2V}$, and Aβ1–42$_{MIX}$ solutions were analyzed at final concentrations of 100 μM in 50 mM phosphate buffer, pH 7.4, at 22 °C by parallel and independent static and dynamic laser light scattering (SLS and DLS). The homemade LLS apparatus is described elsewhere (40). The average scattered intensity (SLS) readily reveals the emergence and growth of aggregates in solution, starting from monomers, as it is proportional to the square of the molecular mass of the scattering particles. The correlation function of the scattered intensity (measured by DLS) yielded the translational diffusion coefficients of particles in solution and then their average hydrodynamic diameter via the Stokes-Einstein relation. DLS data analysis was carried out using the method of cumulants, suitable to detect the evolution of the weight-average hydrodynamic size of particles in solution, and the non-negative least squares method (41), to determine their size distribution at different incubation times.

Small Angle X-ray Scattering (SAXS)—To obtain information on size, homogeneity, and shape of the Aβ peptide oligomers in solution on a local scale, we employed SAXS. Measurements were performed at the high brilliance ID02 beamline of European Synchrotron Radiation Facility (Grenoble, France) with a beam cross-section of 0.3 × 0.8 mm and wavelength of 0.1 nm in the region of momentum transfer, $q = (2\pi/\lambda)\cdot\sin(\theta/2)$, 0.017 $nm^{-1} \leq q \leq 4.65\ nm^{-1}$, where θ is the scattering angle. Plastic capillaries (KI-beam, ENKI) were mounted horizontally onto a six-place sample holder allowing for nearly simultaneous measurements on sample and reference cells in the same environmental conditions. Samples were prepared as described for LLS analysis, and all measurements were performed at 22 °C. The exposure time of each measurement was very short, 0.1 s, to minimize any possible radiation damage. Several frames were collected on each sample, with 1-s sleeping times, carefully compared, and mediated if superimposable within experimental error. The measured SAXS profiles report the scattered radiation intensity as a function of the momentum transfer, q. Several spectra relative to the empty cells and the solvent were taken, carefully compared, and subtracted from each sample spectrum. To investigate a wide q-region, spectra relative to different q-ranges were compared and joined.

Fluorescence Emission Spectroscopy—Fluorescence spectroscopy was carried out using two specific probes, 1-anilino-8-naphthalene-sulfonate (ANS) and 4,4′-dianilino-1,1′-binaphthyl-5,5′-disulfonic acid (Bis-ANS) (Sigma), to detect hydrophobicity in oligomer preparation at neutral pH, to probe high hydrophobic sites, and to monitor conformational changes. Fluorescence measurements were carried out on an LS50B Luminescence Spectrometer (PerkinElmer Life Sciences) using a quartz cuvette with a 1-cm light path. Thirty μl of each oligomeric solution was added to 300 μl of 30 mM citrate buffer, pH 2.4, containing 25 μM ANS or Bis-ANS, and the fluorescence intensity was immediately recorded in the range of 400–600-nm emission wavelengths and with an excitation wavelength of 386 nm (42). The analysis was performed on three/four replicates for each sample. Fluorescence was also acquired in the absence of Aβ1–42 oligomers.

Circular Dichroism (CD)—Aβ1–42 oligomers were analyzed immediately after their dilution to the final concentration of 25 μM in μM phosphate buffer, pH 7.4, to avoid signal saturation in the spectra. The CD spectra were recorded on a Jasco J-815 spectropolarimeter (Jasco, Easton, MD) at 4 °C from 190 to 260 nm (1.0-nm bandwidth and 0.1-nm resolution) using a 0.1-cm path length quartz cell. Generally, a sensitivity of 100 millidegrees, a response of 4 s, a scan speed of 50 nm/min, and 5 accumulations were used. Spectrum of appropriate buffer was subtracted from the Aβ1–42 spectra, and CD spectra were expressed as mean molar ellipticity (Φ).

Statistical Analysis—Means with standard error or standard deviation and one-way analysis of variance followed by Tukey's analysis were performed using Prism GraphPad software, Version 6.01 (GraphPad Software, Inc.).

RESULTS

Electron Microscopy Analysis of Aβ1–42 Oligomeric Assemblies—The temporal window for the formation of oligomers during the aggregation process was analyzed. Comparative EM analyses between Aβ1–42$_{WT}$ and Aβ1–42$_{A2V}$ revealed the prevalence of two different structures. Aβ1–42$_{WT}$ showed a predominant presence of globulomers with a size in the range of 15–40 nm and few annular structures with a size of about 60 nm (Fig. 1, *A* and *D*), whereas Aβ1–42$_{A2V}$ was highly enriched with annular structures in the range of 7–70 nm (Fig. 1*B* and *E*), suggesting that the presence of the A2V mutation promoted a distinctive oligomerization pathway. As shown at higher magnification (Fig. 1*E*), Aβ1–42$_{A2V}$ annular aggregates had an electron-dense core that may suggest the formation of a pore where uranyl acetate solution was accumulated. The annular structures formed by Aβ1–42$_{A2V}$ continued the oligomerization process, as shown by the neoformed extension (see the *inset* of Fig. 1*E*). The co-incubation of Aβ1–42$_{WT}$ and Aβ1–42$_{A2V}$ was characterized by a morphology highly resembling the Aβ1–42$_{WT}$ peptide alone, with the presence of many globulomers and annular structures with smaller dimensions in the range of 9–25 nm (Fig. 1, *C* and *F*).

Atomic Force Microscopy Analysis of Aβ1–42 Oligomers—Peptides were analyzed immediately after the switching procedure and after incubation for 24 h at 4 °C. Freshly prepared solutions contained only monomeric assemblies, whereas samples that underwent incubation disclosed the presence of small oligomers of different sizes (data not shown). SPIP software was used to analyze the distribution of oligomer population in terms of diameters (Fig. 2*A*) and heights (Fig. 2, *B–D*). This software enables the elaboration of AFM images, and it specifically takes into account the features of the tips and the tapping mode. Therefore, it is able to obtain very accurate data on the height and diameter of the molecular assemblies formed by Aβ peptides (43). The cumulative frequency graph (Fig. 2*A*) reports the diameter distribution. Aβ1–42$_{WT}$ produced a family of oligomers with a range of highly defined dimension, the majority (65%) being between 5 and 20 nm in diameter, and no oligomeric aggregates larger than 60 nm were detected. Aβ1–42$_{A2V}$ produced an evenly distributed population of oligomers (>90%) in the range of 20–70 nm with scattered structures reaching 140–180 nm. The co-incubation of Aβ1–42$_{WT}$ and Aβ1–42$_{A2V}$ did not generate aggregated structures larger than 60 nm, and most oligomers were in the range of 10–50

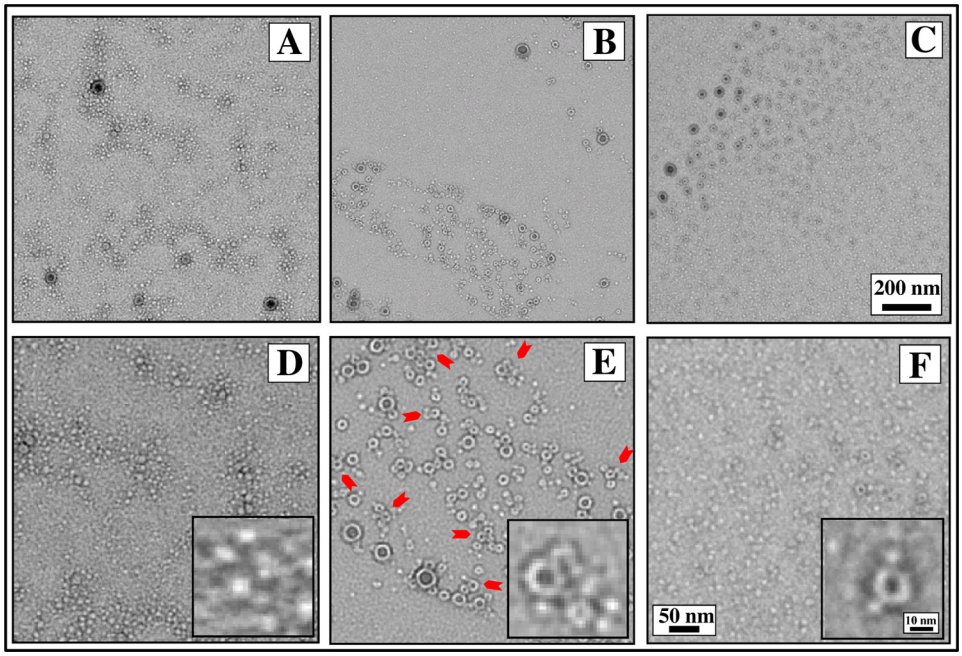

FIGURE 1. **EM analysis of Aβ1–42$_{WT}$, Aβ1–42$_{A2V}$, and Aβ1–42$_{MIX}$.** EM micrographs of 100 μM Aβ1–42$_{WT}$ (*panels A* and *D*), Aβ1–42$_{A2V}$ (*panels B* and *E*), and Aβ1–42$_{MIX}$ (*panels C* and *F*) incubated in 50 mM phosphate buffer, pH 7.4, for 24 h at 4 °C. The *inset* in *panel E* shows a detail of the micrograph at high resolution. The *red arrows* point to annular structures formed by Aβ1–42$_{A2V}$ showing a neoformed extension as an indication of oligomerization process progression. The micrographs are representative of a minimum of 10 different areas.

nm. This indicates a much lower propensity to oligomerization for the Aβ1–42$_{MIX}$ than for Aβ1–42$_{WT}$ or Aβ1–42$_{A2V}$ (Fig. 2*A*, Table 1).

The same samples were also analyzed to determine oligomer height distribution (Fig. 2, *B–D*, and Table 1). As reported in Table 1, the means of the oligomer heights were similar for all samples. However, as reported in Figs. 2, *B–D*, it can be noticed that the main peak of the frequency distribution is sharper for Aβ1–42$_{WT}$ assemblies (90% ≤1 nm in heights).

Fluorescence Spectral Characterization of Aβ Oligomer Conformation—All oligomeric preparations were examined for their pattern of exposure of hydrophobic and hydrophilic residues using an ANS assay. This dye enables the orientation of aromatic side chains or the definition of formation and disruption of organized hydrophobic patches and clefts to be defined. It is well known that the binding of ANS to the exposed hydrophobic clusters of a protein results in both an increased intensity of the fluorescence emission of the dye and a blue shift in the maximum emission wavelength. Significant differences in fluorescence emission was only seen between Aβ1–42$_{WT}$ and Aβ1–42$_{A2V}$ as an indication of the presence of more hydrophobic residues on the external surface of Aβ1–42$_{A2V}$ (Fig. 3, *A* and *B*). Moreover, Aβ1–42$_{A2V}$ showed a shift in its maximum emission wavelength from ~500 nm (referred to Aβ1–42$_{WT}$) to ~491 nm (Fig. 3*C*).

The same samples were then tested for the presence of soluble oligomeric forms with a α-helical or random coil/mixed conformers by Bis-ANS assay (Fig. 3*A*). This probe does not emit fluorescence in the presence of fibrillar structures. Aβ1–42$_{A2V}$ produced a significantly higher fluorescence signal than Aβ1–42$_{WT}$ or Aβ1–42$_{MIX}$, indicating a greater amount of oligomeric assemblies conformers with a α-helical or random coil/mixed. It is important to note that the co-incubation of Aβ1–42$_{WT}$ and Aβ1–42$_{A2V}$ led to molecular assemblies closely resembling those of Aβ1–42$_{WT}$. We also determined the absence of fibrillar assemblies in all three experimental groups using the classical thioflavin T assay (data not shown). As confirmatory information, a CD technique was used to determine the secondary structure of Aβ oligomers. CD spectra of Aβ1–42$_{WT}$, Aβ1–42$_{A2V}$, and Aβ1–42$_{MIX}$ oligomeric solutions did not show significant differences, and they evidenced a predominant random-coil conformation with a negative peak in the signal around 195–197 nm (Fig. 4).

Short-time Kinetics of Aβ Assembly Determined via Laser Light Scattering—The initial stages of aggregation of Aβ peptides were also followed by SLS and DLS measurements. The change in molecular assemblies in 100 μM peptide solutions kept at 22 °C was followed for 24 h.

Because the scattered intensity is proportional to the square of the particle mass, this technique is sensitive to the presence of preformed seeds with high molecular weight. If non-negligible in number, the contribution of seeds to the total scattered intensity dominates and hides the contribution of the small particles. In our case, immediately after the switching procedure, the initial states of Aβ1–42 peptides were distinctly monomeric, allowing the first steps of aggregation to be followed. Experimental results are shown in Figs. 5 and 6 reporting, respectively, SLS and DLS observations.

For all Aβ1–42 species, aggregation started immediately in solutions, leading to the rapid formation of oligomers in coexistence with a population of monomers with average hydrodynamic radii of 2–3 nm. In fact, looking at Fig. 6 one can appreciate that the size distribution, mainly monomeric at the beginning (0.1 h), has evolved to include a population of oligomers after 3 h. The oligomeric aggregates were slightly different in size, being larger for Aβ1–42$_{WT}$ (about 35 nm) than for

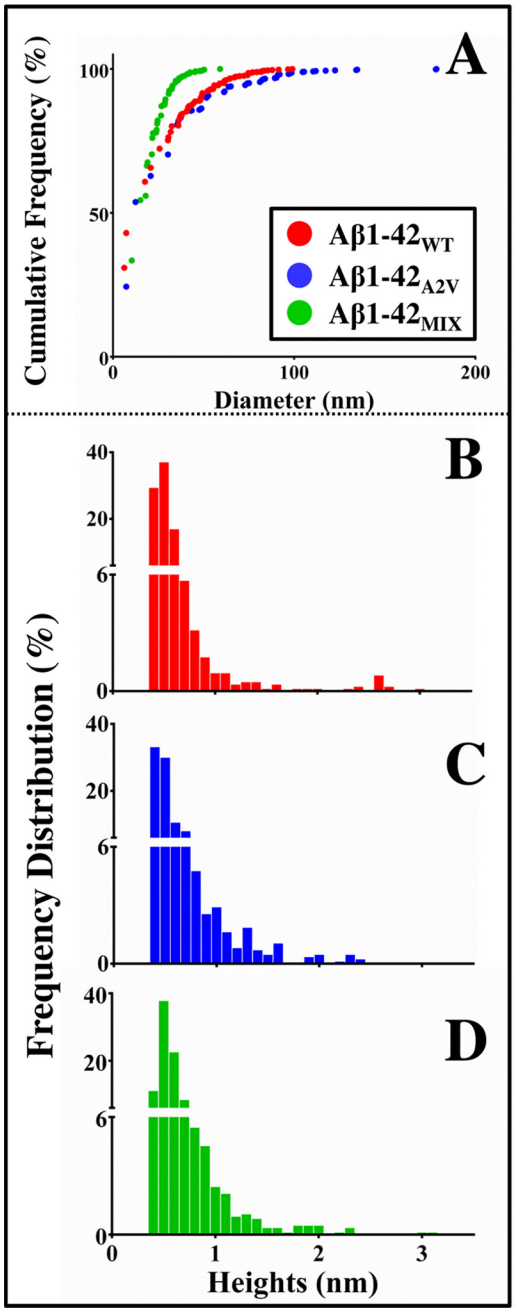

FIGURE 2. **Diameters and heights of Aβ1–42$_{WT}$, Aβ1–42$_{A2V}$, and Aβ1–42$_{MIX}$.** SPIP analysis of Aβ1–42$_{WT}$, Aβ1–42$_{A2V}$, and Aβ1–42$_{MIX}$ oligomers was observed by AFM. *A*, oligomer diameter distribution reported as a cumulative frequency graph; *B–D*, oligomer heights of Aβ1–42$_{WT}$ (*B*), Aβ1–42$_{A2V}$ (*C*), and Aβ1–42$_{MIX}$ (*D*) reported as a frequency distribution graph.

Aβ1–42$_{MIX}$ and Aβ1–42$_{A2V}$ (average hydrodynamic radius of 25 nm). Moreover, although the earliest kinetics of oligomer formation and their initial size distribution were quite similar for the three peptides, remarkable differences were observed in the following 24 h. During the 24-h time-course, the aggregation of Aβ1–42$_{WT}$ and Aβ1–42$_{MIX}$ was characterized by a two-step process: (i) the prompt formation of early oligomers and (ii) a delayed slower aggregation, starting after a time lag of several hours (~6 h), as shown in *panel B* of Fig. 5. The fitting curves for the second aggregation step, also shown in Fig. 5*B*, were obtained by $I(t) = I_{final}\ (1 - e^{-t/\tau})$, where I_{final} is the asymptotic value of the scattered intensity, and τ is the characteristic time. Aβ1–42$_{MIX}$ displayed a slightly longer lag time (t_{MIX} = 8.6 h) with respect to Aβ1–42$_{WT}$ (t_{WT} = 6.7 h) and a slower characteristic time (τ_{WT} = 1.7 h, τ_{MIX} = 3 h). This indicates that the aggregation process proceeded more slowly for the Aβ1–42$_{MIX}$. Moreover the asymptotic intensity value I_{final} is lower for the Aβ1–42$_{MIX}$ (Fig. 5*C*). The increase in scattered intensity for both solutions could not be attributed to a simple increase in the number of oligomers because the average hydrodynamic radius of particles also migrated toward larger values. Monomers are progressively hidden by the overwhelming scattered intensity contributed by oligomers. In fact, they progressively increased in number over 24 h. This is shown in Fig. 6 where the size distribution after 24 h is reported. Notably, at this interval of time, all oligomeric species were still soluble.

Reversely, in the Aβ1–42$_{A2V}$ solution, the oligomer population readily appeared just after dissolution as shown in Fig. 6, where the initial distribution (0.1 h) reveals the presence of a small fraction of aggregates. All over, Aβ1–42$_{A2V}$ follows a different path for aggregation as compared with Aβ1–42$_{WT}$ and Aβ1–42$_{MIX}$. In fact, after <2 h, an additional population appeared with a much larger size, as readily revealed by SLS, showing a huge spike in the scattered intensity as reported in *panel A* of Fig. 5. The sudden rise in intensity is connected to the formation of fibrils, very few in numbers and tending to precipitate and adhere to cell walls. Meanwhile, oligomeric species were also still present as the majority. Their time evolution was difficult to follow; nonetheless they preserved their solubility even after 24 h as seen in Fig. 6. The mutated peptide sequence had an intrinsic tendency to form rapidly structured oligomers.

Small Angle X-ray Scattering: Structural Elucidation of Aβ1–42 Aggregates—To obtain information on the structure of Aβ1–42 aggregates on a local scale, we performed small angle x-ray scattering measurements just after switching and after 3 h at 22 °C. This late peptide solution displays an oligomer composition similar to that found after 24 h at 4 °C (data not shown). Fig. 7 reports the SAXS intensity spectra obtained at 0.1- and 3-h delays in the momentum transfer range 0.017 $nm^{-1} \leq q \leq 4.65\ nm^{-1}$ for the three peptides.

In the high q-region, the spectra of the three different systems are superimposable and can be fitted with the form factor of very small nuclei of condensation of about 1.3 nm in size. The size of small particles is compatible with the presence of Aβ1–42 monomers in all samples at both delays.

In the low-q region, the short-delay spectra can be fitted with the form factor of rod-like structures, as usually found for polymers and peptides, for the three peptides. This may indicate the onset of self-assembly of monomers up to a persistence length of tens of nm in agreement with laser light scattering measurements. The spectra collected 3 h later indicate that, besides monomers, more structured forms are present in solutions at that delay. In the case of Aβ1–42$_{A2V}$ SAXS spectrum, the characteristic slope of a packed polymer network ($q^{-1.7}$) (44) indicates that the Aβ1–42$_{A2V}$ aggregates are not compact globular or rod-like structures but rather look like disperse assembly of particles with branched-type features. After 3 h, Aβ1–42$_{WT}$ and Aβ1–42$_{MIX}$ also showed connected structures, which did

TABLE 1

Diameters and heights of Aβ1–42$_{WT}$, Aβ1–42$_{A2V}$, and Aβ1–42$_{MIX}$

The table shows the outcome of SPIP analysis of 100 μM peptide solutions in 50 mM phosphate buffer and incubated at 4 °C for 24 h. Statistical analysis among the groups was done with one-way analysis of variance followed by Tukey's multiple comparisons test. SPIP analysis was done on a minimum of five different areas. NS, not significant.

	Aβ1–42$_{WT}$	Aβ1–42$_{A2V}$	Aβ1–42$_{MIX}$	Statistical analysis
		Mean ± S.D.		
Diameter (nm)	21.43 ± 18.19	25.58 ± 23.37	18.23 ± 8.34	WT *vs.* A2V[a] WT *vs.* MIX[a] A2V *vs.* MIX[a]
Height (nm)	0.58 ± 0.33	0.62 ± 0.31	0.65 ± 0.30	WT *vs.* A2V[b] WT *vs.* MIX[a] A2V *vs.* MIX[b]

[a] $p < 0.0001$.
[b] NS, not shown.

not recruit all the material, as can be inferred by the milder slopes of the intensity decays reported in Fig. 7. Notably, Aβ1–42$_{MIX}$ displayed the lowest degree of supramolecular complexation.

DISCUSSION

A673V mutation differs from other genetic alterations in the amyloid precursor protein sequence because of its recessive inheritance traits. An A673V homozygous carrier presented with early onset dementia characterized by an aggressive cortico-subcortical atrophy and subcortical white matter changes (45). Distinctive neuropathological features were the morphology, composition, and topology of Aβ deposits, which were of large size, mostly perivascular, and exhibited a complete correspondence between the pattern elicited by amyloid staining and the labeling obtained with anti Aβ antibodies (46). The amyloid deposits were predominantly composed by Aβ1–40 and were also abundant in the cerebellum, at variance with sporadic AD (46). The A673V mutation enhances Aβ production and significantly increases the fibrillogenic properties of Aβ. However, the interaction of Aβ1–42$_{WT}$- and Aβ1–42$_{A2V}$-mutated peptides inhibits Aβ folding (45, 47). These findings are consistent with the observation that the A673V heterozygous carriers do not develop the disease and offer grounds for the development of a novel therapy for sporadic AD based on modified peptides homologous to residues 1–6 of Aβ carrying the A2V substitution (47). The strength of this approach, as compared with strategies based on purely theoretical grounds or large screening strategies, is that the A2V Aβ variant occurs in humans and prevents the development of disease when present in the heterozygous state (47).

We focused our interests on the molecular assembly of Aβ1–42 peptides to understand the biochemical reasons of the influence of A673V mutation in Aβ1–42 folding, the higher toxicity, and the protective effect seen in the heterozygous state. We investigated the early stages of the Aβ folding process after the formation of oligomeric structures, which are considered key toxic species in the onset and progression of AD pathogenesis.

We report here a qualitative and quantitative analysis of Aβ oligomer formation by Aβ1–42$_{WT}$, Aβ1–42$_{A2V}$, and Aβ1–42$_{MIX}$ to unveil the features of different oligomer populations formed over time. Morphological structural analysis of Aβ1–42$_{A2V}$ revealed the prevalent formation of annular structures. Lashuel *et al.* (13) showed that mutant amyloid proteins associated with familial AD (Arctic mutation) and familial Parkinson disease (α-synuclein mutants A53T and A30P) form morphologically indistinguishable annular assemblies that resemble a class of pore-forming bacterial toxins, suggesting that inappropriate membrane permeabilization might be the cause of cell dysfunction and even cell death in amyloid diseases (13). Under our experimental conditions, the oligomers formed by the Aβ1–42$_{A2V}$ also showed the presence of annular structures as deduced by the presence of uranyl acetate solution in the sample analyzed by EM. In fact, unlike Aβ1–42$_{WT}$, Aβ1–42$_{A2V}$ formed annular structures wrapped around a wettable trapping central spot. This suggests that the hydrophilic residues of Aβ1–42$_{A2V}$ may be preferentially located in the center, with a corresponding disposition of the hydrophobic residues on the external rim or on the top and bottom sides of the annulus. These structures were almost absent in the case of Aβ1–42$_{WT}$ where globulomers were the most abundant population. The co-incubation of Aβ1–42$_{WT}$ and Aβ1–42$_{A2V}$ produced an intermediate morphological condition consisting of both globulomers and annular structures. Interestingly, AFM characterization of Aβ1–42$_{MIX}$ assemblies showed the presence of oligomers with a smaller average size, suggesting that Aβ1–42$_{MIX}$ has a much lower propensity to oligomerization than Aβ1–42$_{WT}$ or Aβ1–42$_{A2V}$ alone.

Kinetic comparison between Aβ1–42$_{A2V}$ and Aβ1–42$_{WT}$ showed that the former proceeded along a different pathway of structured oligomer formation. The key role was played by the first step, which was the formation of early assemblies that led to the formation of Aβ assemblies after a very efficient dock-and-lock mechanism (48–50).

When comparing Aβ1–42$_{MIX}$ with Aβ1–42$_{WT}$, results showed that the route leading to the formation of oligomers in Aβ1–42$_{WT}$, characterized by the formation of "early" oligomers, followed by a slow additional aggregation was dissimilar to the one observed in the case of Aβ1–42$_{MIX}$ where the second process of aggregation was less extensive and even slower. This was confirmed by LLS analysis of Aβ1–42$_{MIX}$ that had a slightly longer lag time (t_{MIX} = 8.6 h) with respect to Aβ1–42$_{WT}$ (t_{WT} = 6.7 h) and a slower characteristic time (τ_{WT} = 1.7 h *versus* τ_{MIX} = 3 h).

Spectral analysis by fluorescence probes showed that Aβ1–42$_{MIX}$ assemblies closely resembled to those of Aβ1–42$_{WT}$ (Bis-ANS assay) with an intermediary exposure of hydrophobic residues (ANS assay). Aβ1–42$_{A2V}$ oligomers were characterized by the maximum hydrophobicity, confirming the existence of a hydrophilic core and an increase of the hydrophobic resi-

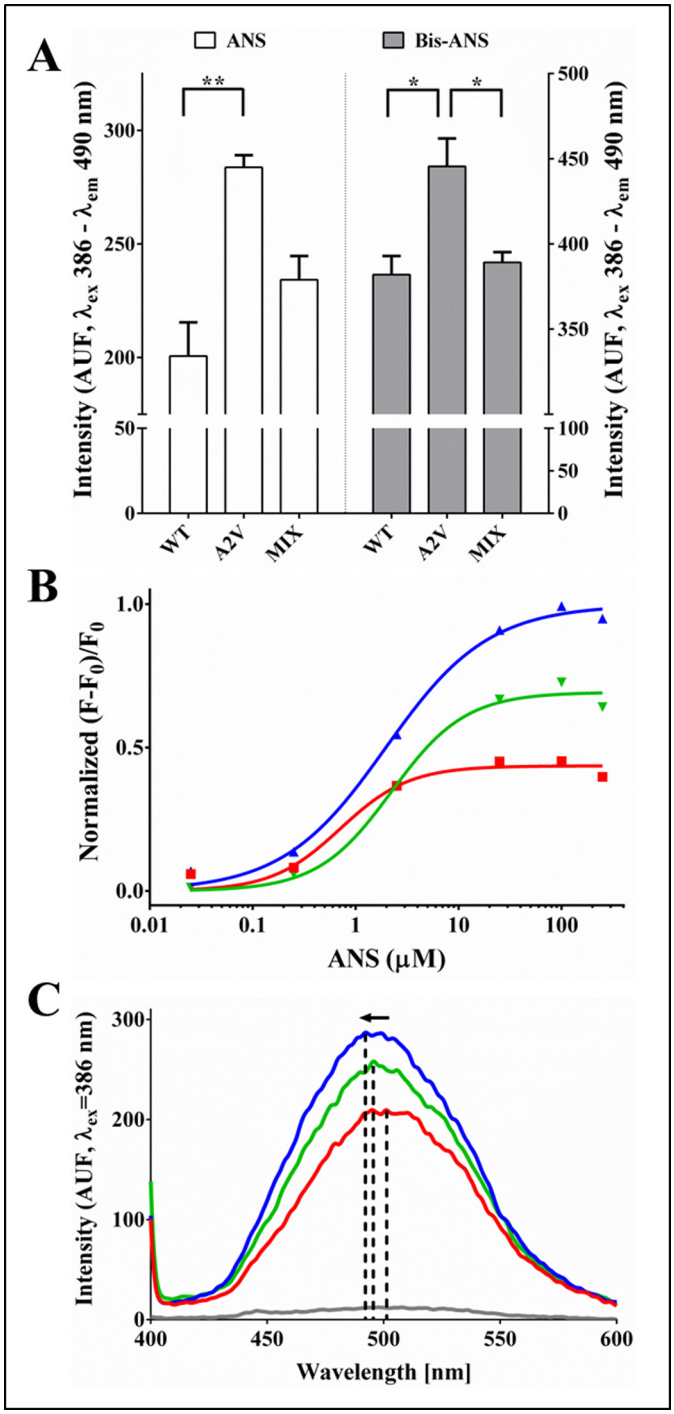

FIGURE 3. **Binding of fluorescent hydroscopic probes.** *A*, binding of fluorescent hydrophobic probes ANS (*left*) and Bis-ANS (*right*) to Aβ1–42$_{WT}$, Aβ1–42$_{A2V}$, and Aβ1–42$_{MIX}$ assemblies. Aβ1–42 oligomers were prepared after incubation of 100 μM concentrations of peptides in phosphate buffer at 4 °C for 24 h. Peptide oligomers were added to a solution containing 25 μM ANS or Bis-ANS, and the fluorescence intensities were immediately recorded using excitation and emission wavelengths of 386 and 490 nm, respectively. *Error bars* are the means ± S.E. for three or four samples. Statistical analysis among the groups was done with the one-way analysis of variance followed by Tukey's multiple comparisons test (*, $p < 0.05$; **, $p < 0.01$). *AUF*, arbitrary unit of fluorescence. *B*, concentration dependence of ANS binding to Aβ peptides. Normalized ratio between the total area under the fluorescence emission spectra of ANS in the presence ($F - F_o$) and absence (F_o) of Aβ1–42 oligomers. The lines represent the best-fitting curve of Aβ1–42$_{WT}$ (*red*), Aβ1–42$_{A2V}$ (*blue*), and Aβ1–42$_{MIX}$ (*green*) data. *C*, ANS fluorescence emission spectra of phosphate buffer (*gray*), Aβ1–42$_{WT}$ (*red*), Aβ1–42$_{A2V}$ (*blue*), and Aβ1–42$_{MIX}$ (*green*) assemblies. Oligomer samples were added to a solution containing 100 μM ANS, and the fluorescence intensities were immediately recorded using excitation and emission wavelengths of 386 and 400–600 nm, respectively. The spectra are representative of three to four samples. The *black arrow* indicates the blue shift in the maximum emission wavelength.

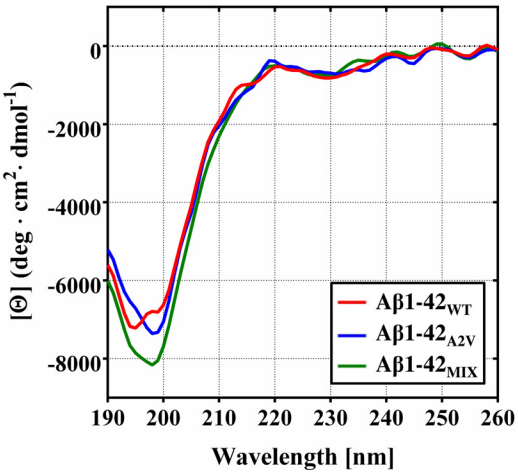

FIGURE 4. **CD analysis of Aβ1–42$_{WT}$, Aβ1–42$_{A2V}$, and Aβ1–42$_{MIX}$.** Oligomers were prepared after incubation of 100 μM Aβ1–42 peptides in 50 mM phosphate solution, pH 7.4, at 4 °C for 24 h. Then peptide solutions were diluted to final concentrations of 25 μM in the same buffer and analyzed. All measurements were performed at 4 °C, and 5 accumulations were used. CD spectra were expressed as mean molar ellipticity (Φ).

dues on the external surface, as detected by ANS assay. To this regard, Mannini *et al.* (51, 52) reported that the exposure of hydrophobic residues on the surface of aberrant protein oligomers increases the toxicity of oligomeric structures, enabling a major interaction with cell membranes.

In terms of local structural organization SAXS analysis indicated that, as expected for a point mutation, the individual structural unit is the same for the three peptides. Nonetheless, their spatial arrangement in the structured oligomers was different. The transition from rod-like to more structured aggregates was more extensive and prompts in Aβ1–42$_{A2V}$ and clearly occurred via the formation of interconnected networks. The Aβ1–42$_{MIX}$ resulted in aggregates with the lowest degree of supramolecular complexation with respect to Aβ1–42$_{WT}$ and Aβ1–42$_{A2V}$, suggesting a negative interference in the supramolecular organization.

In conclusion, we demonstrated that the A2V mutation is able to promote a peculiar oligomerization process pathway of Aβ1–42 that leads to the formation of annular structures with a higher hydrophobicity profile and, hence, toxicity as also observed in an *in vivo* model (53). When the heterozygous condition was reproduced, the aggregation effect of the A2V mutation was lost, confirming that its effect is present only when in homozygosity one. Interestingly, Aβ1–42$_{MIX}$ not only was less prone to aggregate when compared with mutated alone, but also it produced smaller aggregates when compared with the wild type sequence as well. This suggests that the mutation in the heterozygous state is able to hinder the aggregation process and generates unstable structures. This is in good agreement with our previous observations showing that aggregates formed by an equimolar mixture of Aβ1–42$_{WT}$ and Aβ1–42$_{A2V}$ were far more unstable than those generated by either Aβ1–42$_{WT}$ or Aβ1–42$_{A2V}$ (45). This is most likely the biochemical basis of the

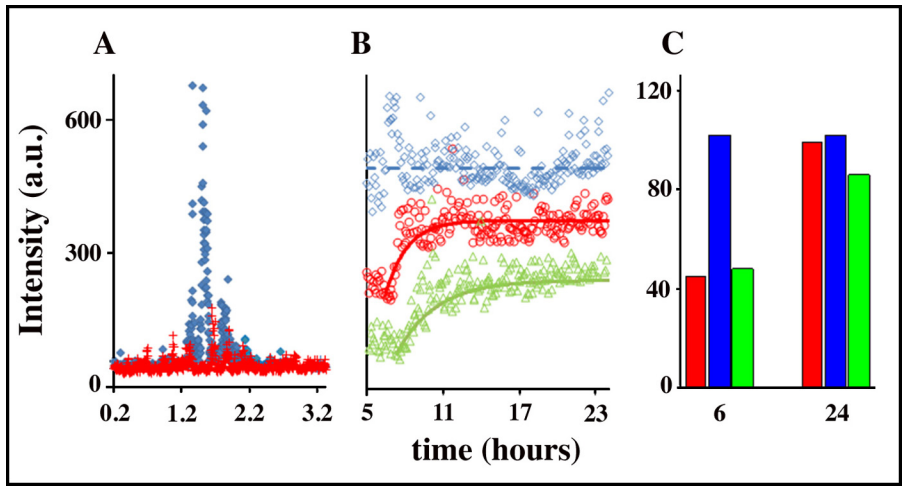

FIGURE 5. **Kinetics of formation of aggregates of Aβ1–42 peptides as determined by SLS.** *A*, a huge spike dominates the time evolution of the intensity scattered by Aβ1–42$_{A2V}$ at ~1.5 h from switching, well before the onset of the delayed slow aggregation regime found for Aβ1–42$_{MIX}$ and Aβ1–42$_{WT}$, also reported for comparison. *a.u.*, absorbance units. *B*, time evolution of the light intensity scattered by different Aβ solutions after 6 h from dissolution. Curves are arbitrarily shifted vertically for better visibility. Colors identify Aβ1–42$_{WT}$ (*red*), Aβ1–42$_{A2V}$ (*blue*), and Aβ1–42$_{MIX}$ (*green*). This behavior was observed after a time lag from switching and is indicative of delayed slow aggregation. Delay is slightly longer for Aβ1–42$_{MIX}$ (t_{MIX} = 8.6 h) than for Aβ1–42$_{WT}$ (t_{WT} = 6.7 h). *Lines* are the corresponding exponential fits, $I(t) = I_{final}(1 - e^{-t/\tau})$, where I_{final} is the asymptotic scattered intensity, also reported in *panel C* together with the starting values. Fitting curves could be determined only for Aβ1–42$_{WT}$ and Aβ1–42$_{MIX}$, with characteristic times τ_{WT} = 1.7 h and τ_{MIX} = 3 h. A *dashed line* in *panel B* marks the average scattered intensity of Aβ1–42$_{A2V}$ in this time interval, showing a different behavior.

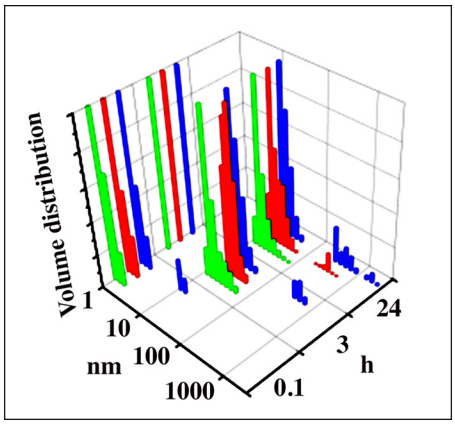

FIGURE 6. **Size distribution of aggregates of Aβ1–42 peptides as determined by DLS.** Volume-weighted size distributions of aggregates of Aβ1–42 peptides at three different delays from switching, namely, 0.1, 3, and 24 h. Colors identify Aβ1–42$_{WT}$ (*red*), Aβ1–42$_{A2V}$ (*blue*), and Aβ1–42$_{MIX}$ (*green*).

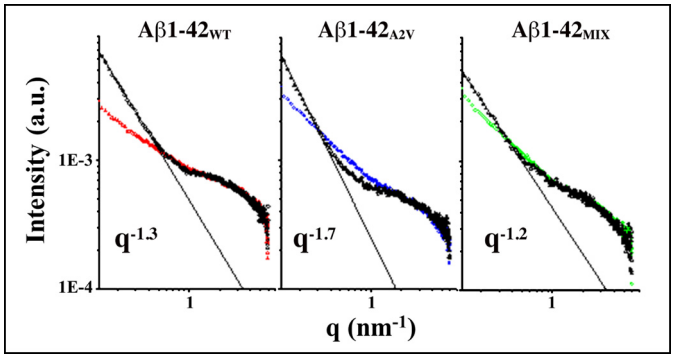

FIGURE 7. **Small angle x-ray scattering studies of Aβ1–42.** SAXS intensity spectra in the log-log scale of Aβ1–42$_{WT}$ (*left panel*) Aβ1–42$_{A2V}$ (*central panel*), and Aβ1–42$_{MIX}$ (*right panel*) at two different delays: 0.1 h (*colored*), 3 h (*black*). Linear slopes correspond to different q^{-S} intensity decays. For Aβ1–42$_{A2V}$ the slope $q^{-1.7}$ is characteristic for a network of connected polymers. *a.u.*, absorbance units.

protective effect shown by the A673V mutation in the heterozygous carrier.

The second remarkable point evidenced in this work was the critical role played by the N-terminal region in the Aβ molecular assembly. In fact, in the homozygous condition the A2V mutation led to aggregation while on the other hand in the heterozygous state the evolution and kinetics of the aggregation process was hindered. This latter phenomenon was driven by the Aβ1–42$_{A2V}$ peptide difficulty in forming stable intermolecular interactions with the wild type sequence.

Acknowledgments—The critical reading of the manuscript by Dr. Claudia Manzoni is gratefully acknowledged. We are grateful to ID02 beamline staff and T. Narayanan at the European Synchrotron Radiation Facility (Grenoble, France) for technical assistance. Flamma Spa, Bergamo, Italy kindly provided FMOC amino acids for peptide synthesis.

REFERENCES

1. Mayeux, R., and Stern, Y. (2012) Epidemiology of Alzheimer disease. *Cold Spring Harb. Perspect. Med.* **2,** a006239
2. Serrano-Pozo, A., Frosch, M. P., Masliah, E., and Hyman, B. T. (2011) Neuropathological alterations in Alzheimer disease. *Cold Spring Harb. Perspect. Med.* **1,** a006189
3. Lambert, M. P., Barlow, A. K., Chromy, B. A., Edwards, C., Freed, R., Liosatos, M., Morgan, T. E., Rozovsky, I., Trommer, B., Viola, K. L., Wals, P., Zhang, C., Finch, C. E., and Krafft, G. A. (1998) Diffusible, nonfibrillar ligands derived from Aβ1–42 are potent central nervous system neurotoxins. *Proc. Natl. Acad. Sci. U.S.A.* **95,** 6448–6453
4. Hartley, D. M., Walsh, D. M., Ye, C. P., Diehl, T., Vasquez, S., Vassilev, P. M., Teplow, D. B., and Selkoe, D. J. (1999) Protofibrillar intermediates of amyloid β-protein induce acute electrophysiological changes and progressive neurotoxicity in cortical neurons. *J. Neurosci.* **19,** 8876–8884
5. Walsh, D. M., Klyubin, I., Fadeeva, J. V., Cullen, W. K., Anwyl, R., Wolfe, M. S., Rowan, M. J., and Selkoe, D. J. (2002) Naturally secreted oligomers of amyloid β protein potently inhibit hippocampal long-term potentiation *in vivo*. *Nature* **416,** 535–539
6. Walsh, D. M., Klyubin, I., Fadeeva, J. V., Rowan, M. J., and Selkoe, D. J.

(2002) Amyloid-β oligomers: their production, toxicity, and therapeutic inhibition: soluble Aβ and AD natural Aβ oligomers inhibit hippocampal long-term potentiation. *Biochem. Soc. Trans.* **30,** 552–557
7. Hardy, J., and Selkoe, D. J. (2002) The amyloid hypothesis of Alzheimer's disease: progress and problems on the road to therapeutics. *Science* **297,** 353–356
8. Walsh, D. M., Hartley, D. M., Kusumoto, Y., Fezoui, Y., Condron, M. M., Lomakin, A., Benedek, G. B., Selkoe, D. J., and Teplow, D. B. (1999) Amyloid β-protein fibrillogenesis: structure and biological activity of protofibrillar intermediates. *J. Biol. Chem.* **274,** 25945–25952
9. Bitan, G., Kirkitadze, M. D., Lomakin, A., Vollers, S. S., Benedek, G. B., and Teplow, D. B. (2003) Amyloid β-protein (Aβ) assembly: Aβ40 and Aβ42 oligomerize through distinct pathways. *Proc. Natl. Acad. Sci. U.S.A.* **100,** 330–335
10. Gong, Y., Chang, L., Viola, K. L., Lacor, P. N., Lambert, M. P., Finch, C. E., Krafft, G. A., and Klein, W. L. (2003) Alzheimer ' s disease-affected brain: presence of oligomeric Aβ ligands (ADDLs) suggests a molecular basis for reversible memory loss. *Proc. Natl. Acad. Sci. U.S.A.* **100,** 10417–10422
11. Deshpande, A., Mina, E., Glabe, C., and Busciglio, J. (2006) Different conformations of amyloid β induce neurotoxicity by distinct mechanisms in human cortical neurons. *J. Neurosci.* **26,** 6011–6018
12. Caughey, B., and Lansbury, P. T. (2003) Protofibrils, pores, fibrils, and neurodegeneration: separating the responsible protein aggregates from the innocent bystanders. *Annu. Rev. Neurosci.* **26,** 267–298
13. Lashuel, H. A., Hartley, D., Petre, B. M., Walz, T., and Lansbury Jr., P. T. (2002) Amyloid pores from pathogenic mutations. *Nature* **418,** 291
14. Hoshi, M., Sato, M., Matsumoto, S., Noguchi, A., Yasutake, K., Yoshida, N., and Sato, K. (2003) Spherical aggregates of β-amyloid (amylospheroid) show high neurotoxicity and activate Tau protein kinase I/glycogen synthase kinase-3β. *Proc. Natl. Acad. Sci. U.S.A.* **100,** 6370–6375
15. Roychaudhuri, R., Yang, M., Hoshi, M. M., and Teplow, D. B. (2009) Amyloid β-protein assembly and Alzheimer disease. *J. Biol. Chem.* **284,** 4749–4753
16. Borreguero, J. M., Urbanc, B., Lazo, N. D., Buldyrev, S. V., Teplow, D. B., and Stanley, H. E. (2005) Folding events in the 21–30 region of amyloid β-protein (Aβ) studied *in silico*. *Proc. Natl. Acad. Sci. U.S.A.* **102,** 6015–6020
17. Baumketner, A., Bernstein, S. L., Wyttenbach, T., Lazo, N. D., Teplow, D. B., Bowers, M. T., and Shea, J. E. (2006) Structure of the 21–30 fragment of amyloid β-protein. *Protein Sci.* **15,** 1239–1247
18. Cruz, L., Rao, J. S., Teplow, D. B., and Urbanc, B. (2012) Dynamics of metastable β-hairpin structures in the folding nucleus of amyloid β-protein. *J. Phys. Chem. B* **116,** 6311–6325
19. Cruz, L., Urbanc, B., Borreguero, J. M., Lazo, N. D., Teplow, D. B., and Stanley, H. E. (2005) Solvent and mutation effects on the nucleation of amyloid β-protein folding. *Proc. Natl. Acad. Sci. U.S.A.* **102,** 18258–18263
20. Urbanc, B., Cruz, L., Yun, S., Buldyrev, S. V., Bitan, G., Teplow, D. B., and Stanley, H. E. (2004) *In silico* study of amyloid β-protein folding and oligomerization. *Proc. Natl. Acad. Sci. U.S.A.* **101,** 17345–17350
21. Fawzi, N. L., Phillips, A. H., Ruscio, J. Z., Doucleff, M., Wemmer, D. E., and Head-Gordon, T. (2008) Structure and dynamics of the Aβ (21–30) peptide from the interplay of NMR experiments and molecular simulations. *J. Am. Chem. Soc.* **130,** 6145–6158
22. Lazo, N. D., Grant, M. A., Condron, M. C., Rigby, A. C., and Teplow, D. B. (2005) On the nucleation of amyloid β-protein monomer folding. *Protein Sci.* **14,** 1581–1596
23. Lee, C., and Ham, S. (2011) Characterizing amyloid-β protein misfolding from molecular dynamics simulations with explicit water. *J. Comput. Chem.* **32,** 349–355
24. Chen, W., Mousseau, N., and Derreumaux, P. (2006) The conformations of the amyloid-β (21–30) fragment can be described by three families in solution. *J. Chem. Phys.* **125,** 084911
25. Lam, A. R., Teplow, D. B., Stanley, H. E., and Urbanc, B. (2008) Effects of the arctic (E^{22}→G) mutation on amyloid β-protein folding: discrete molecular dynamics study. *J. Am. Chem. Soc.* **130,** 17413–17422
26. Scheidt, H. A., Morgado, I., Rothemund, S., and Huster, D. (2012) Dynamics of amyloid β fibrils revealed by solid-state NMR. *J. Biol. Chem.* **287,** 2017–2021
27. Selkoe, D. J. (2001) Alzheimer's disease: genes, proteins, and therapy. *Physiol. Rev.* **81,** 741–766
28. Tai, L. M., Bilousova, T., Jungbauer, L., Roeske, S. K., Youmans, K. L., Yu, C., Poon, W. W., Cornwell, L. B., Miller, C. A., Vinters, H. V., Van Eldik, L. J., Fardo, D. W., Estus, S., Bu, G., Gylys, K. H., and Ladu, M. J. (2013) Levels of soluble apolipoprotein E/amyloid-β (Aβ) complex are reduced and oligomeric Aβ increased with APOE4 and Alzheimer disease in a transgenic mouse model and human samples. *J. Biol. Chem.* **288,** 5914–5926
29. Tai, L. M., Mehra, S., Shete, V., Estus, S., Rebeck, G. W., Bu, G., and LaDu, M. J. (2014) Soluble apoE/Aβ complex: mechanism and therapeutic target for APOE4-induced AD risk. *Mol. Neurodegener.* **9,** 2–14
30. Hardy, J. A., and Higgins, G. A. (1992) Alzheimer's disease: the amyloid cascade hypothesis. *Science* **256,** 184–185
31. Ferreira, S. T., and Klein, W. L. (2011) The Aβ oligomer hypothesis for synapse failure and memory loss in Alzheimer's disease. *Neurobiol. Learn. Mem.* **96,** 529–543
32. Beeg, M., Stravalaci, M., Bastone, A., Salmona, M., and Gobbi, M. (2011) A modified protocol to prepare seed-free starting solutions of amyloid-β (Aβ)1–40 and Aβ1–42 from the corresponding depsipeptides. *Anal. Biochem.* **411,** 297–299
33. Stravalaci, M., Bastone, A., Beeg, M., Cagnotto, A., Colombo, L., Di Fede, G., Tagliavini, F., Cantù, L., Del Favero, E., Mazzanti, M., Chiesa, R., Salmona, M., Diomede, L., and Gobbi, M. (2012) Specific recognition of biologically active amyloid-β oligomers by a new surface plasmon resonance-based immunoassay and an *in vivo* assay in *Caenorhabditis elegans*. *J. Biol. Chem.* **287,** 27796–27805
34. Coin, I. (2010) The depsipeptide method for solid-phase synthesis of difficult peptides. *J. Pept. Sci.* **16,** 223–230
35. Taniguchi, A., Sohma, Y., Hirayama, Y., Mukai, H., Kimura, T., Hayashi, Y., Matsuzaki, K., and Kiso, Y. (2009) "Click peptide": pH-triggered *in situ* production and aggregation of monomer Aβ1–42. *Chembiochem.* **10,** 710–715
36. Balducci, C., Beeg, M., Stravalaci, M., Bastone, A., Sclip, A., Biasini, E., Tapella, L., Colombo, L., Manzoni, C., Borsello, T., Chiesa, R., Gobbi, M., Salmona, M., and Forloni, G. (2010) Synthetic amyloid-β oligomers impair long-term memory independently of cellular prion protein. *Proc. Natl. Acad. Sci. U.S.A.* **107,** 2295–2300
37. Sclip, A., Arnaboldi, A., Colombo, I., Veglianese, P., Colombo, L., Messa, M., Mancini, S., Cimini, S., Morelli, F., Antoniou, X., Welker, E., Salmona, M., and Borsello, T. (2013) Soluble Aβ oligomers-induced synaptopathy: c-Jun N-terminal kinase's role. *J. Mol. Cell Biol.* **5,** 277–279
38. Manzoni, C., Colombo, L., Bigini, P., Diana, V., Cagnotto, A., Messa, M., Lupi, M., Bonetto, V., Pignataro, M., Airoldi, C., Sironi, E., Williams, A., and Salmona, M. (2011) The molecular assembly of amyloid ab controls its neurotoxicity and binding to cellular proteins. *Plos ONE* **6,** e24909
39. Manzoni, C., Colombo, L., Messa, M., Cagnotto, A., Cantù, L., Del Favero, E., and Salmona, M. (2009) Overcoming synthetic Aβ peptide aging: a new approach to an age-old problem. *Amyloid* **16,** 71–80
40. Lago, P., Rovati, L., Cantù, L., and Corti, M. (1993) A quasielastic light scattering detector for chromatographic analysis. *Rev. Sci. Instrum.* **64,** 1797–1802
41. Lawson, C. L., and Hanson, R. J. (1995) *Solving Least Squares Problems*, Vol. 15, Society for Industrial and Applied Mathematics, Philadelphia, PA
42. LeVine, H., 3rd (2002) 4,4′-Dianilino-1,1′-binaphthyl-5,5′-disulfonate: report on non-β-sheet conformers of Alzheimer's peptide β(1–40). *Arch. Biochem. Biophys.* **404,** 106–115
43. Munz, M. (2013) Microstructure and roughness of photopolymerized poly(ethyleneglycol) diacrylate hydrogel as measured by atomic force microscopy in amplitude and frequency modulation mode. *Appl. Surf. Sci.* **279,** 300–309
44. Lindner, P., and Zemb, T. (2002) *Neutrons, X-rays, and Light: Scattering Methods Applied to Soft Condensed Matter*, 1st Ed., pp. 391–420, North-Holland Delta Series, Amsterdam, ND
45. Di Fede, G., Catania, M., Morbin, M., Rossi, G., Suardi, S., Mazzoleni, G., Merlin, M., Giovagnoli, A. R., Prioni, S., Erbetta, A., Falcone, C., Gobbi, M., Colombo, L., Bastone, A., Beeg, M., Manzoni, C., Francescucci, B., Spagnoli, A., Cantù, L., Del Favero, E., Levy, E., Salmona, M., and Tagliavini, F.

(2009) A recessive mutation in the APP gene with dominant-negative effect on amyloidogenesis. *Science* **323,** 1473–1477
46. Giaccone, G., Morbin, M., Moda, F., Botta, M., Mazzoleni, G., Uggetti, A., Catania, M., Moro, M. L., Redaelli, V., Spagnoli, A., Rossi, R. S., Salmona, M., Di Fede, G., and Tagliavini, F. (2010) Neuropathology of the recessive A673V APP mutation: Alzheimer disease with distinctive features. *Acta Neuropathol.* **120,** 803–812
47. Di Fede, G., Catania, M., Morbin, M., Giaccone, G., Moro, M. L., Ghidoni, R., Colombo, L., Messa, M., Cagnotto, A., Romeo, M., Stravalaci, M., Diomede, L., Gobbi, M., Salmona, M., and Tagliavini, F. (2012) Good gene, bad gene: new APP variant may be both. *Prog. Neurobiol.* **99,** 281–292
48. Gobbi, M., Colombo, L., Morbin, M., Mazzoleni, G., Accardo, E., Vanoni, M., Del Favero, E., Cantù, L., Kirschner, D. A., Manzoni, C., Beeg, M., Ceci, P., Ubezio, P., Forloni, G., Tagliavini, F., and Salmona, M. (2006) Gerstmann-Sträussler-Scheinker disease amyloid protein polymerizes according to the "dock-and-lock" model. *J. Biol. Chem.* **281,** 843–849
49. Maggio, J. E., Stimson, E. R., Ghilardi, J. R., Allen, C. J., Dahl, C. E., Whitcomb, D. C., Vigna, S. R., Vinters, H. V., Labenski, M. E., and Mantyh, P. W. (1992) Reversible *in vitro* growth of Alzheimer disease β-amyloid plaques by deposition of labeled amyloid peptide. *Proc. Natl. Acad. Sci. U.S.A.* **89,** 5462–5466
50. Esler, W. P., Stimson, E. R., Jennings, J. M., Vinters, H. V., Ghilardi, J. R., Lee, J. P., Mantyh, P. W., and Maggio, J. E. (2000) Alzheimer's disease amyloid propagation by a template-dependent dock-lock mechanism. *Biochemistry* **39,** 6288–6295
51. Campioni, S., Mannini, B., Zampagni, M., Pensalfini, A., Parrini, C., Evangelisti, E., Relini, A., Stefani, M., Dobson, C. M., Cecchi, C., and Chiti, F. (2010) A causative link between the structure of aberrant protein oligomers and their toxicity. *Nat. Chem. Biol.* **6,** 140–147
52. Mannini, B., Cascella, R., Zampagni, M., van Waarde-Verhagen, M., Meehan, S., Roodveldt, C., Campioni, S., Boninsegna, M., Penco, A., Relini, A., Kampinga, H. H., Dobson, C. M., Wilson, M. R., Cecchi, C., and Chiti, F. (2012) Molecular mechanisms used by chaperones to reduce the toxicity of aberrant protein oligomers. *Proc. Natl. Acad. Sci. U.S.A.* **109,** 12479–12484
53. Diomede, L., Di Fede, G., Romeo, M., Bagnati, R., Ghidoni, R., Fiordaliso, F., Salio, M., Rossi, A., Catania, M., Paterlini, A., Benussi, L., Bastone, A., Stravalaci, M., Gobbi, M., Tagliavini, F., and Salmona, M. (2014) Expression of A2V-mutated Aβ in C. elegans results in oligomer formation and toxicity. *Neurobiol. Dis.* **62,** 521–532